International Journal of Greenhouse Gas Control 119 (2022) 103733

Contents lists available at ScienceDirect

International Journal of Greenhouse Gas Control

journal homepage: www.elsevier.com/locate/ijggc

Dawsonite as a Temporary but Effective Sink for Geological Carbon Storage

Peng Lu [a,*], Guanru Zhang [b,c], Yi Huang [b], John Apps [d], Chen Zhu [c]

[a] EXPEC Advanced Research Center, Saudi Aramco, Dhahran 31311, Saudi Arabia
[b] College of Ecology and Environment, Chengdu University of Technology, Chengdu 610059, China
[c] Department of Earth and Atmospheric Sciences, Indiana University, Bloomington, IN 47405, USA
[d] Earth and Environmental Sciences Area, Lawrence Berkeley National Laboratory, Berkeley, CA 94705, USA

ARTICLE INFO

Keywords:
Dawsonite
Mineral trapping
Carbon capture and storage
Reactive transport modeling

ABSTRACT

The possibility of using dawsonite mineral trapping as a carbon capture and storage (CCS) strategy intrigues many. In this study, we used a dawsonite-rich (~10%) CO_2 gas reservoir in the Hailar basin in northern China as a natural analogue of a CO_2 storage site, along with numerical modeling, to demonstrate that a large amount of dawsonite can be generated in sandstone formations, provided sufficient Na-rich feldspar and CO_2 gas are available. While precipitated dawsonite can be preserved only in a hydrodynamically-closed system in the long term under high CO_2 fugacity and $\log((Na^+)/(H^+))$ activities in solution, short-term trapping of CO_2 in dawsonite (on the order of 10 kyr) is possible and lowers CO_2 pressure, which mitigates the risk of CO_2 leakage to the ground surface or overlying drinking water aquifers. The re-dissolution of dawsonite after a few thousand years facilitates progressive dissipation of the gas phase CO_2 over time. Consideration of reservoirs or saline aquifers with minerals or formation water that can provide a high abundance of dissolved sodium, significantly increases the number of potential CCS sites globally. Furthermore, alternating water-and-gas injection regimens could enhance the precipitation of dawsonite in Na-rich aquifers. Future editions of the Carbon Storage Atlas should consider aquifer geochemistry in the site selection for secure long-term carbon storage in addition to the volumetric considerations for short-term operation.

1. Introduction

Mineral trapping is recognized as the most secure carbon capture and storage (CCS) mechanism to ensure the long-term retention of carbon dioxide following its injection into permeable porous geologic formations (Bachu et al., 1994). This process can immobilize CO_2 as carbonates, typically as calcite, dolomite, ankerite, and siderite, through interaction with pre-existing host-rock minerals containing divalent Mg^{2+}, Ca^{2+}, or Fe^{2+}, and replicates in some respects the immobilization of CO_2 generated during petroleum maturation in organic-rich sedimentary formations (Coudrain-Ribstein et al., 1998; Lu et al., 2020). Under some natural conditions, however, dawsonite ($NaAl(OH)_2CO_3$) is also stabilized, sometimes attaining significant volume fractions (VF) over 0.2 in some sedimentary formations that may originally have been rich in sodic feldspars (Du,1982; Wopfner and Höcker, 1987; Baker et al., 1995; Moore at al., 2005; Worden, 2006; Gao et al., 2009; Liu et al., 2011, Uysal et al., 2011; Comerio et al., 2014; Yu et al., 2014; Zhou et al., 2014; Yu et al., 2015; Li and Li, 2016; Li et al.,2017; 2018; Ming et al., 2017; Király et al., 2018; Zhao et al., 2018; Yu et al., 2020; Qu et al., 2022 and Cseresznyés et al., 2021). Analogous presumed sodic feldspar-rich or arkosic sedimentary formations could therefore be very favorable targets for CCS. However, the relative infrequency of observed dawsonite occurrences, especially when compared with its relatively common appearance as a thermodynamically stable phase in comparable geochemical modeling, has invited speculation that both its formation and persistence may be determined principally by kinetic factors, e.g., Hellevang et al. (2005, 2011, 2014), or influenced by host rock composition and the competitive formation of metastable phases, e.g., Takaya et al. (2019), rather than by thermodynamic stability. In particular, Hellevang et al. (2005) cautioned that dawsonite formed during supercritical CO_2 injection, as predicted by extant modeling (Johnson et al., 2004; Xu et al., 2004; 2005; 2010; Cantucci, et al., 2009; Liu et al., 2011a; 2011b; Okuyama et al., 2013; Shabani et al., 2022; Yu et al., 2015; Zhang et al., 2015; 2016; Yang et al., 2017; Zhu et al., 2019) would dissolve following CO_2 dissipation, which is sometimes misinterpreted to discount its value for CO_2 mineral trapping. Considerable uncertainty remains as to precisely under what conditions dawsonite can form and persist in geological formations to the extent needed to

* Corresponding author:
E-mail address: peng.lu@aramco.com (P. Lu).

https://doi.org/10.1016/j.ijggc.2022.103733
Received 15 February 2022; Received in revised form 8 June 2022; Accepted 12 July 2022
Available online 21 July 2022

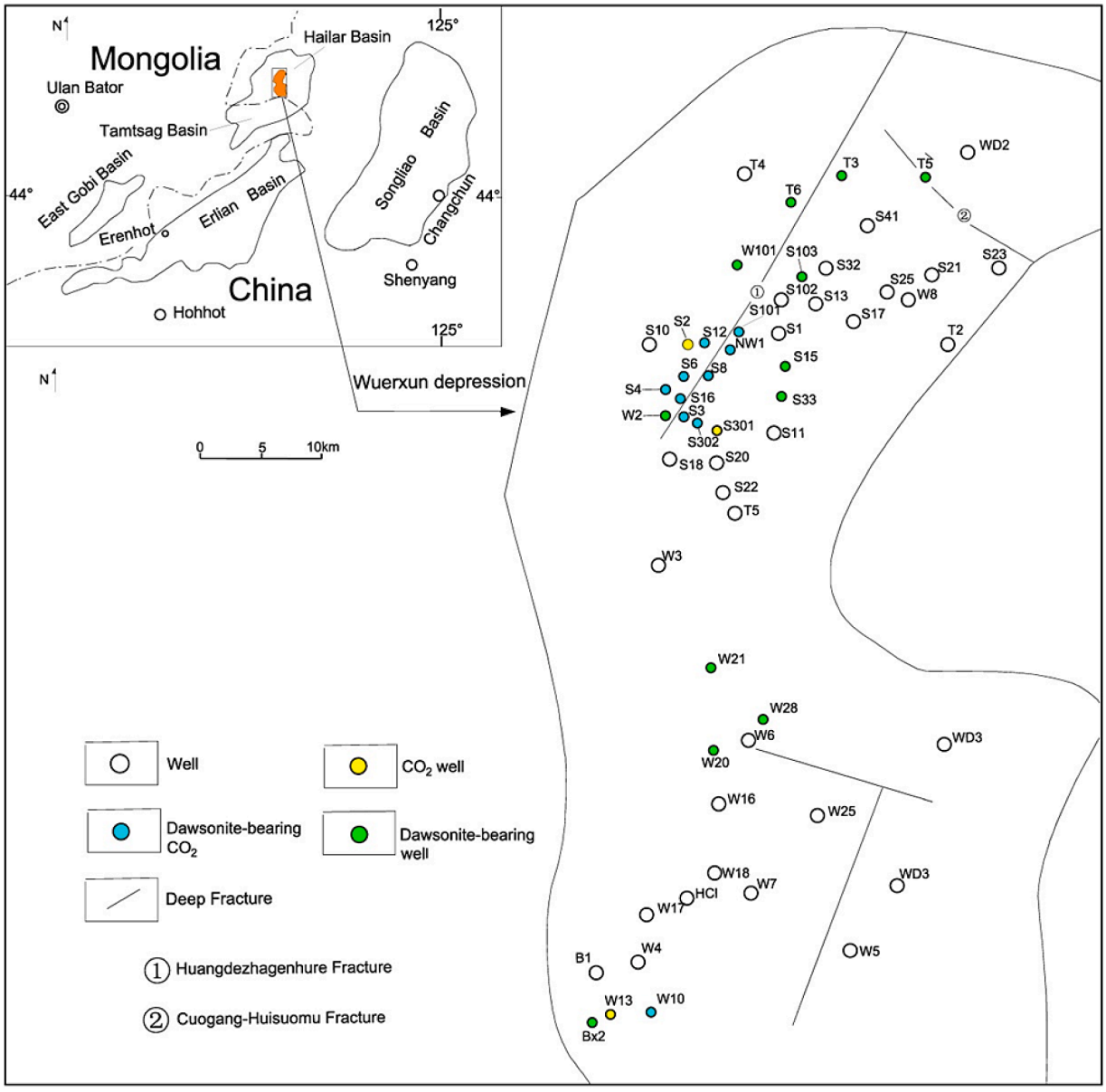

Fig. 1. Location of Haiar basin and distribution of dawsonite and CO_2, and deep fractures (after Gao et al., 2009).

meet CCS objectives, given the complex interplay of fluid flow, geochemical interactions, and reactive transport rates. Due consideration is therefore given to these uncertainties in the modeling described in this paper.

For CCS, the time scale of interest is hundreds to thousands of years (IPCC, 2005). Transitory dawsonite precipitation and persistence within this time scale can be beneficial because it would lower CO_2 partial pressure in the system and thus decrease the risk of leakage. How long it would take before dawsonite were to precipitate and how long it could persist in a leaky reservoir depend on the chemical reactivity of the host rocks to high-pressure CO_2, the nucleation, precipitation, and dissolution rates of dawsonite, and the hydraulic connectivity and dynamics of the aquifer. Even if, as seems probable, dawsonite were to dissolve completely if CO_2 was to leak away (Hellevang et al., 2005), its transient trapping of CO_2 would still be beneficial for CO_2 storage. As discussed further in a later section of this paper, *Issues Relating to Dawsonite Nucleation and Growth*, circumstantial evidence suggests that a significant induction time must elapse before dawsonite would nucleate and precipitate following saturation, thereby rendering impractical any confirmatory laboratory or field tests. Reactive transport modeling, despite many inherent limitations, must therefore be employed in order to gain insight into the significance and timing of the participating processes and their sensitivity to parameter variations. In this contribution, we focus specifically on the processes affecting mineral trapping of CO_2 by dawsonite in sedimentary formations where dawsonite deposition could be substantive. Furthermore, by recognizing current model and parameter uncertainties relating to the rates of dawsonite nucleation, precipitation, and dissolution, we encompass a range of conditions where dawsonite precipitation would be significant for CCS, a task that has been insufficiently explored until now.

We first replicate the natural formation of dawsonite in the Hailar basin of northeastern China with a two-dimensional reactive transport simulation. This model of a natural analogue permits direct comparison with the predicted formation of dawsonite mineral assemblages expected under CO_2 injection rates in potential CCS repositories. For comparison, we superimposed environmental conditions analogous to those of the Sleipner CCS project (Audigane, et al., 2007; Gaus et al., 2005; Zhang et al., 2016) upon the stratigraphy and architecture of the

Table 1
Main simulation scenarios in this study.

Case	Parameter				
	Albite volume fraction	Regional groundwater flow	Reservoir architecture	Time scale	CO_2 injection
Base Case	0.172	no	Based on K1n2 formation in Hailar basin	15 Myr	2.3×10^{-7} kg/s (15 Myr)
CCS Case 1, 2, 3	0.02	0, 0.1, 1 m/yr	Expanded the Base Case domain to the right to form an anticlinal structure	10 kyr	2.4×10^{-3} kg/s (100 yr)
CCS Case 4[§]	SAA	no	SAA	SAA	SAA
CCS Case 5	SAA	no	SAA	SAA	2.4×10^{-3} kg/s +1.75 x 10^{-2} kg/s water (100 yr)
CCS Case 6	0.172	no	SAA	SAA	2.4×10^{-3} kg/s (100 yr)
CCS Case 7-10[#]	SAA	no	SAA	SAA	SAA

[§] In CCS Case 4 dawsonite precipitation was not allowed.
All other parameters were the same as CCS Case 1.
[#] CCS Case 7 used Burton–Cabrera–Frank (BCF) rate law (Burton et al., 1951) for dawsonite precipitation and a rate constant two orders of magnitude lower than CCS Case 1.
In CCS Case 8, dawsonite precipitation rate constant was two orders of magnitude lower than CCS Case 1.
In CCS Case 9, dawsonite precipitation rate constant was two orders of magnitude higher than CCS Case 1.
In CCS Case 10, BCF rate law was used for dawsonite precipitation dawsonite precipitation rate constant was two orders of magnitude higher than CCS Case 1.
All other parameters were the same as CCS Case 1. SAA = Same as above.

previously modeled Hailar Basin aquifer and elaborated on this comparison through additional simulations reflecting plausible alternative CCS scenarios. In this way, we could assess the role dawsonite plays in the geochemical evolution of injected CO_2, thereby placing dawsonite trapping in its proper perspective.

2. Geological background

The Hailar basin is located in northeastern China, north of the Tamsag Basin, near the Mongolian border (Gao et al., 2009) (Fig. 1). The stratigraphy of the Hailar basin is described in previous studies (Gao et al., 2009; Zhou et al., 2014). A CO_2 reservoir is located in the Late Cretaceous Nantun Formation (K1n2), which is a dawsonite-bearing sandstone. Carbon and helium isotope signatures ($\delta^{13}C$ CO_2: -11.4‰ to -8.2‰; $^3He/^4He$ isotopic ratios: 1.68 x 10^{-6} to 2.08 x 10^{-6}), the high abundance of CO_2 (> 90%), and igneous rock occurrences in the underlying strata suggest a possible mantle-CO_2 component (Gao et al., 2009) that invaded K1n2 via the Wuxi fault system. However, it is uncertain whether the present CO_2 has the same source as that which entered the formation about 110-85 Ma ago, as determined by isotope geochemistry, fluid inclusion, and diagenetic sequence studies, further constrained by hydrocarbon charging history and illite K/Ar ages (Gao et al., 2009; Zhou et al., 2014). The Hailar basin has optimal geological conditions that facilitate the long-term preservation of dawsonite: (1) two overlying confining mudstone formations (Damoguaihe and Yimin formations) with a total thickness of ~ 1,000 m, (2) a semi-anticline-shaped structure to trap CO_2 gas, and (3) a relatively closed hydrodynamic system (Gao et al., 2009; Zhou et al., 2014).

Dawsonite is abundant in the sandstones, ranging from 2% to 22%, averaging 10.8% (Gao et al., 2009), largely coexisting with the CO_2 gas phase in the reservoir (Gao et al., 2009), and having precipitated through CO_2 reaction with formation minerals (Gao, 2007).

3. Methods

Coupled reactive flow and mass transport simulations were conducted using TOUGHREACT V3.0-OMP-ECO2N (Xu et al., 2014). The design of the Base Case is the same as Zhang et al. (2021). We assumed that the depth, thickness, porosity, and permeability of the K1n2 reservoir at ~110-85 Ma were similar to those at present, because of their similar burial depth (Gao et al., 2009). The thickness of the formation is 250 m. We took the bottom and top of the K1n2 formation as the upper and lower boundaries in our model and the fault as the right-hand boundary (**Supporting Information (SI) Section S1**). Considering computational efficiency and availability of well data (S6, S4, and W2), the model was extended ~6,000 m to the left.

Cross-sectional 2-D rectangular grids were set up with a total of 1,500 cells of $100 \times 1 \times 10$ m (X × Y × Z) each. A pressure of 20 MPa was assigned to the 1,830-m depth based on hydrostatic pressure, but the reservoir pressure was allowed to change during the simulation. The formation temperature was assumed to be a constant 90 °C throughout the simulation, in line with the burial-thermal history (Gao et al., 2009). The initial water composition, mineralogical assemblages, boundary conditions, porosity and permeability, and other hydrogeologic, thermodynamic, and kinetic data parameters are listed in **SI Section S1**.

CO_2 was charged at a constant rate (2.3×10^{-7} kg/s) from the bottom of the fault into the K1n2 sandstone. We used reaction kinetics for all minerals but calcite, which was assumed to be in equilibrium with the fluid. The simulation time was 15 Myr, representing ~20 Myr of CO_2 ingress and dawsonite formation (Gao et al., 2009).

The measured dissolution rate of dawsonite is uncertain (Hellevang et al., 2005; 2010). Hellevang et al. (2010) provided 18 data points ranging from 22-77 °C and pH 1.1 -5.0. We separated them into the acidic group (pH 1.1-2.7) and neutral group (4.2-5.0). Then, used the rate constants as a function of temperature to obtain the rate constant at 25 °C and activation energy values for the acidic and neutral mechanisms, respectively, as the input parameters for TOUGHREACT (**SI Section Table S1-4)**. For simulations at the 10 kyr time scale, this uncertain value was mitigated through a sensitivity analysis.

The rate law derived from the principle of detailed balance (Liu et al., 2016) and commonly called the Transition State Theory (TST) rate law in the Earth Science literature (Lasaga, 1981a,b; Aagaard and Helgeson, 1982) has been used for all mineral dissolution and precipitation reactions for the Base Case, except for calcite (set as an equilibrium phase) (**SI Section Table S1-4)**. However, Zhu et al. (2010) indicated that a number of experiments near-equilibrium have shown that the actual relationship between the rates and ΔG_r deviates from this so-called TST linear kinetics. We adopted a non-linear rate law from Alekseyev et al. (1997) for albite dissolution to evaluate the uncertainties caused by rate laws (see **SI, section S6**). The uncertainties of dawsonite precipitation kinetics have been assessed in CCS case 7-10 (see below) because dawsonite kinetics is of greater concern at the CCS time-scale, rather than the million-year time scale.

To explore dawsonite formation and persistence over a 10 kyr period typically anticipated for CCS, we constructed models resembling the mineralogical composition, porosity, and permeability of the Hailar basin, but excluding the fault and with a lower albite VF (CCS Case 1-6; Table 1). The model domain is expanded to the right to form a complete

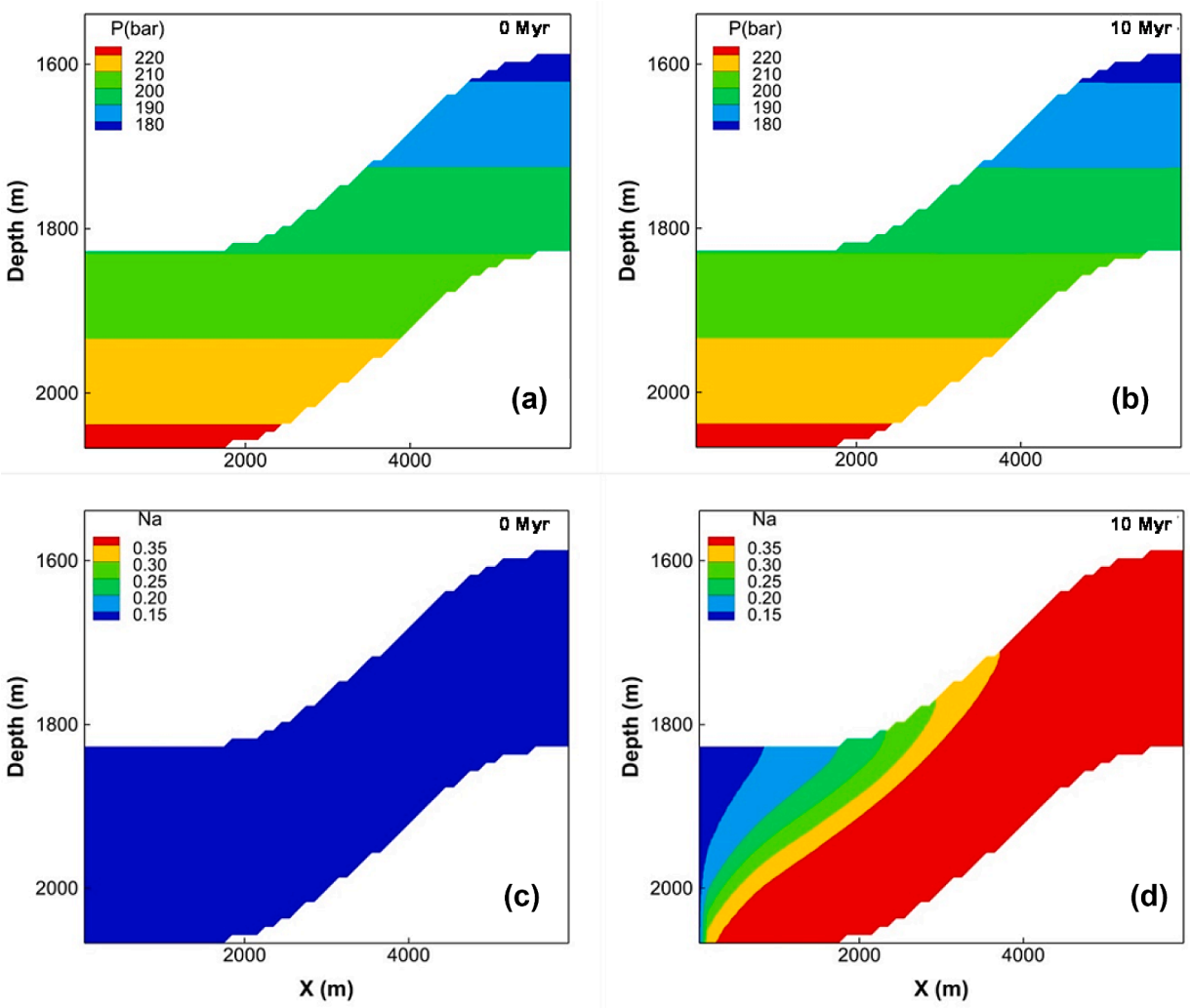

Fig. 2. Simulation results of the Base Case at 0 and 10 Myr. (a) and (b) reservoir pressure (bars; 1 bar = 0.1 MPa); (c) and (d) Na concentration (mol/kgw).

anticlinal structure, which is roughly mirror-symmetrical to the original Hailar architecture with the original right boundary of the Hailar model as the centerline (see **SI, section S7 figures**). Furthermore, the domain was extended 2 km to the left in order to host an extension of HCO_3^- rich water at a high groundwater flow rate (1 m/yr). The albite VF was decreased to ~ 0.02 (3%) to replicate that of the Sleipner CCS project (Hellevang et al., 2010).

In "CCS Case 1-10", the CO_2 injection rate (2.4×10^{-3} kg s^{-1}) was based on the average incursion rate into Layer 9 during 1999-2009 of the Sleipner CCS project (Hellevang et al., 2010). CO_2 injection time is 100 yr and the simulation time 10 kyr. The injection point was at the bottom of the formation at the topmost point of the anticline (see the **SI Section 7**). Regional groundwater (same as initial formation water) was injected from the right boundary at different flow velocities.

In "CCS Case 4", dawsonite precipitation was suppressed to assess the importance of dawsonite trapping during the CCS process. In addition, a water-alternating-with-gas (WAG) case was used to investigate the effects of such an injection scheme on mineral trapping (CCS Case 5). Further details of this process are given in **SI Section 7.**

We consider the albite VF parameter as important. We used the Sleipner 0.02 value for CCS Cases 1-5 and 7-10, and the Hailar 0.172 value for CCS Case 6 to investigate its impact. The simulation parameters for each case are listed in Table 1.

Finally, we included cases using both a lower dawsonite precipitation rate constant and the Burton–Cabrera–Frank (BCF) rate law (Burton et al., 1951) (see the **SI Section 7**) (CCS Case 7), a lower dawsonite precipitation rate constant (CCS Case 8), a higher dawsonite precipitation rate constant (CCS Case 9) and the BCF rate law (CCS Case 10) to evaluate the sensitivity of these parameters on dawsonite precipitation.

4. Results and discussion

4.1. Results from the Base Case (Hailar Basin Natural Analogue)

The temperature was kept at a constant value (90 °C) for the entire reservoir throughout the simulation. Generally, the reservoir pressures show a hydrostatic pressure gradient with the range of ~ 175-225 bars (~ 17.5-22.5 Mpa) (Fig. 2a). Due to the low CO_2 injection rate (2.3×10^{-7} kg/s), there is almost no change in reservoir pressure for the base case (Fig. 2b). However, CO_2 invasion causes substantial salinity changes (the solution is Na-HCO_3 dominated). Na^+ concentrations increase from ~0.13 to ~0.38 mol/kgw at 10 Myr (Figs. 2c and 2d), due to albite dissolution.

After 10 Myr of CO_2 incursion, the system was saturated with dissolved CO_2, and the gas phase appeared at the top of the reservoir with a gas saturation (S_g) of ~0.54 (Fig. 3a). From 10 to 15 Myr, the size of the gas zone increased, and the gas-water contact lay at depths of ~1,600 and ~1,760 m at 10 Myr and 15 Myr, respectively (Figs. 3a, b). The S_g at the top of the reservoir structure was ~0.68 at 15 Myr (Fig. 3b). A spectrum of S_g variations can be seen in the gas zone because of capillary

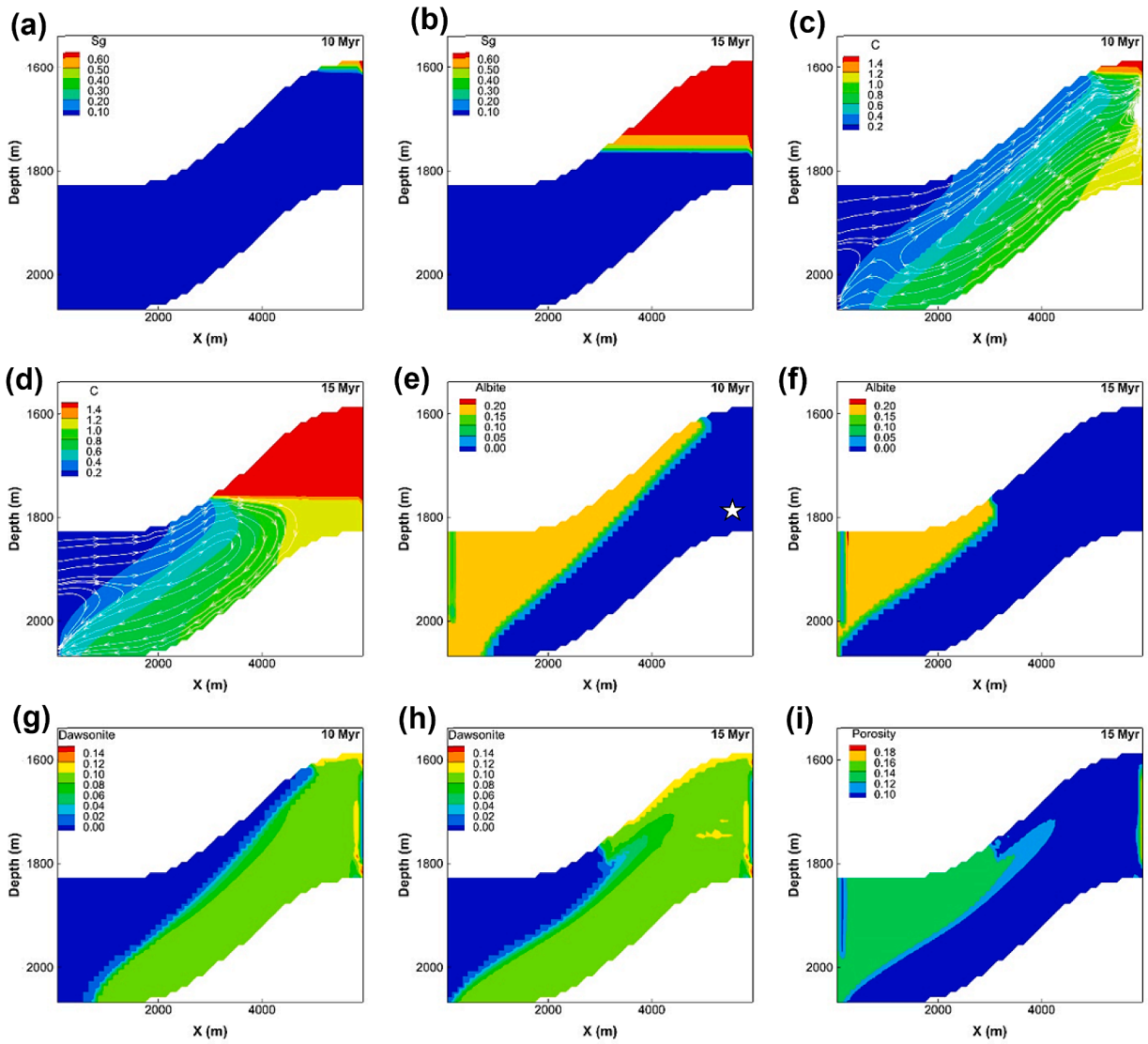

Fig. 3. Simulation results of the Base Case at 10 and 15 Myr. (a) and (b): Spatial distribution of gas saturation (*Sg*). (c) and (d): total dissolved carbon concentration (mol/kgw). The lines with arrows are groundwater streamlines. (e) and (f): albite volume fraction. (g) and (h): dawsonite volume fraction. (i) porosity (VF) at 15 Myr.

effects, similar to that in Zhang et al. (2019).

Total dissolved C increased from 0.06 mol/kg H_2O in the initial formation water to 1.18 mol/kg H_2O near the fault in the lower right part of the reservoir (Fig. 3c). The dissolution of CO_2 into the formation water increased the density of the water, resulting in density-driven convective flow (Figs. 3c, d).

The invaded CO_2 from the fault in the lower right corner dissolved into and acidified the formation water. The water became undersaturated with respect to albite (e.g., the saturation index of albite in the lower right part of the reservoir was -0.94). Conversion of albite to dawsonite occurred in the high C concentration areas (cf. Figs. 3c and 3d). At 10 Myr, albite (initial volume fraction of 0.172) in the lower right part of the reservoir was completely converted to dawsonite and quartz (Figs. 3e, 3g and **Fig. S2-1**). The volume fraction of dawsonite increased from 0 to 0.099. The overall reaction can be written as Eq. 1.

$$CO_2 + H_2O + NaAlSi_3O_8(\text{albite}) = NaAlCO_3(OH)_2(\text{dawsonite}) + 3SiO_2(\text{-quartz}) \quad (1)$$

Albite conversion to dawsonite was the dominant reaction at 0 – 10 Myr (Figs. 3e - h), controlling porosity evolution (the solid volume reduction is 27.3 cm^3 per mole for albite-to-dawsonite conversion). Porosity decreased ~0.03 VF in the dawsonite precipitation zone at 15 Myr (Fig. 3i>).

The evolution of the four trapping mechanisms of CO_2—structural, residual, solubility, and mineral trapping (IPCC, 2005)—is illustrated in Fig. 4a. We did not distinguish structural from residual CO_2 trapping, combining the two as "gas trapping." The percentage of mineral trapping (predominantly dawsonite precipitation) first increased to ~86%, remained above 80% during for 10 Myr, and then decreased during the remaining 10 - 15 Myr, when albite was by then completely dissolved. CO_2 charged during this time is due mainly to gas and solubility trapping. By 15 Myr, the CO_2 trapped by dawsonite was ~65 %. Solubility trapping attained ~25.6 % at 15 Myr. Almost no gas trapping occurred until 10 Myr, but thereafter increased between 10 - 15 Myr, reaching ~9.5 % at 15 Myr.

Comparing the percentages of different trapping mechanisms between Hailar CO_2 gas reservoir and CarbFix project (Snæbjörnsdóttir et al., 2017) indicated that the mineral trapping process is significantly delayed in natural CO_2 reservoir than that in basalt (Figs. 4b). It only requires ~1.2 yr to reach ~50% mineral trapping and ~2 yr to reach ~100%, while it takes ~3,000 yr to reach ~50% mineral trapping in Hailar.

Several test cases were constructed to evaluate the effects of albite dissolution rate constants, rate law, and quartz precipitation rate

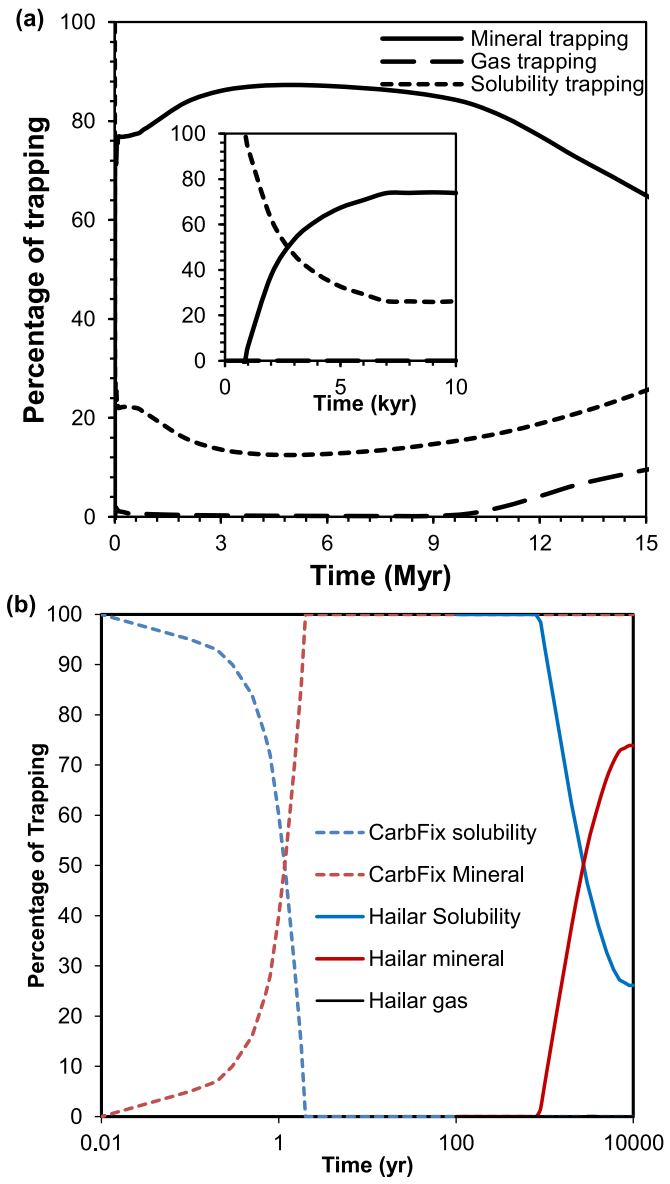

Fig. 4. (a) Percentages of mineral, gas, and solubility trappings as a function of time in the simulated domain of the Base Case. Inset shows the first 10 kyr results (to be compared with CCS cases). Note that the CO_2 lost with density-driven flow from the left boundary is attributed to solubility trapping. (b) Comparison of the percentages of different trapping mechanisms between Hailar CO_2 gas reservoir and CarbFix project (Snæbjörnsdóttir et al., 2017)

constants on dawsonite precipitation in the Hailar basin (see **SI Section S6**). The effects of an increase or decrease of albite and quartz dissolution and precipitation rate constants by two orders of magnitude on CO_2 trapping are within ~±2%. However, mineral trapping was 6% less than the Base Case when using a non-linear rate law (Alekseyev et al., 1997) for albite dissolution.

The simulated spatial distributions of mineral volume fractions of dawsonite, albite, and quartz were generally comparable with observations in the Kln2 Formation (See **SI Section S3** for detailed comparisons), substantiating the credibility of our modeling.

4.2. CCS Simulations, where dawsonite is a temporary CO_2 sink

CCS Cases 1-10 used the verified geochemical model from Hailar, but with modified reservoir architecture and hydraulics to resemble typical CCS formations, such as deep saline aquifers open to groundwater flow. Some simulation results (S_g, C concentration, dawsonite VF) are shown in **SI Section S7**. In all but one case, CCS Case 5 (dawsonite precipitation suppressed), mineral trapping was almost entirely due to dawsonite precipitation.

4.3. Specific CCS Cases

In a closed hydrodynamic system, mineral trapping at 10 kyr was about 37% of the total injected CO_2 in CCS Case 1 (albite VF 0.02), but about 88% in CCS Case 6 (albite VF 0.172) (Fig. 5). For comparison, mineral trapping in the Base Case under natural conditions was 74% at 10 kyr (the inset of Fig. 4). Gas trapping decreased from 77% to 42% and 77% to 0% at 10 kyr in CCS Cases 1 and 6, respectively, due to increased mineral trapping (Fig. 5).

In the case with a groundwater velocity of 0 (CCS Case 1), gas, solubility, and mineral trappings were 44%, 21%, and 35%, respectively (Fig. 5). With a groundwater velocity increased to 0.1 m/y (CCS Case 2), mineral trapping reached a maximum, ~32.3 % at 7 kyr, then decreased gradually to ~29 % between 7-10 kyr. Solubility trapping increased significantly due to groundwater flushing, reaching 51% at 10 kyr. Gas trapping decreased to 20% at 10 kyr. With an unusually high groundwater velocity, e.g., 1 m/yr; CCS Case 3, the maximum amount of mineral trapping was attained at 1 kyr, but at 3 kyr, the dawsonite had completely re-dissolved and mineral trapping decreased to ~0 %, leaving solubility trapping as the dominant mechanism, which reached 100 % after 3 kyr.

If no dawsonite precipitates (CCS Case 4), mineral trapping was almost 0% (Fig. 5), and gas trapping reached ~69.4% at 10 kyr (compared to ~42.3% in CCS Case 1).

Co-injecting CO_2 with water (CCS Case 5) led to greater mineral trapping (43.9% at 10 kyr compared to 37.4% for CCS Case 1) because co-injected water increased the area coverage of the HCO_3^--rich water and the dawsonite precipitation. The area of HCO_3^--rich water in CCS Case 6 was ~ 1.38 times that in the CCS Case 1. Gas trapping was also lower than that in CCS Case 1, indicating a lower risk of leakage.

For the first 100 yr, the patterns for the trapping mechanisms were similar for CCS Cases 1-4 and 6 that mineral trapping was < 1%, gas trapping was ~ 70% and solubility trapping was ~ 30% (Fig. 5). However, for CCS cases 5, gas trapping was ~ 45% and solubility trapping reached ~ 55%.

If the dawsonite precipitation rate was two orders of magnitude higher than previously simulated (CCS Case 9) or by using the Burton–Cabrera–Frank (BCF) (Burton et al., 1951) precipitation rate law (CCS Case 10), the fractions of mineral, gas and solubility trapping were almost identical to those of CCS Case 1 from 0-10 kyr (Fig. 6). If the dawsonite precipitation rate was two orders of magnitude lower (CCS Case 8), the mineral trapping was delayed for ~ 600 yr, but gradually caught up at 10 kyr (Fig. 6). If both the dawsonite precipitation rate was two orders of magnitude lower than previously simulated and BCF precipitation rate law was used (CCS Case 7), the mineral trapping profile was delayed incrementally (~600 yr) without changing its shape (Fig. 6). Mineral trapping under these conditions was also about 2% less at 10 kyr (Fig. 6). The impact of slower dawsonite kinetics was therefore not significant at 10 kyr in our models. Although the dawsonite precipitation rate constant has not been quantitatively measured (Hellevang et al., 2005) and is highly uncertain, modeling indicates that this deficiency is less significant than uncertainties associated with groundwater flow velocities. However, it is critical if the time scale of interest is only 1 kyr, where mineral trapping in CCS case 7 is only ~0.2% (Fig. 6).

4.4. Dawsonite stability

Activity diagrams are useful in investigating the stability of dawsonite in relation to co-existing minerals (Hellevang et al., 2005, Hellevang et al., 2011) (Fig. 7). We extracted the data from a point

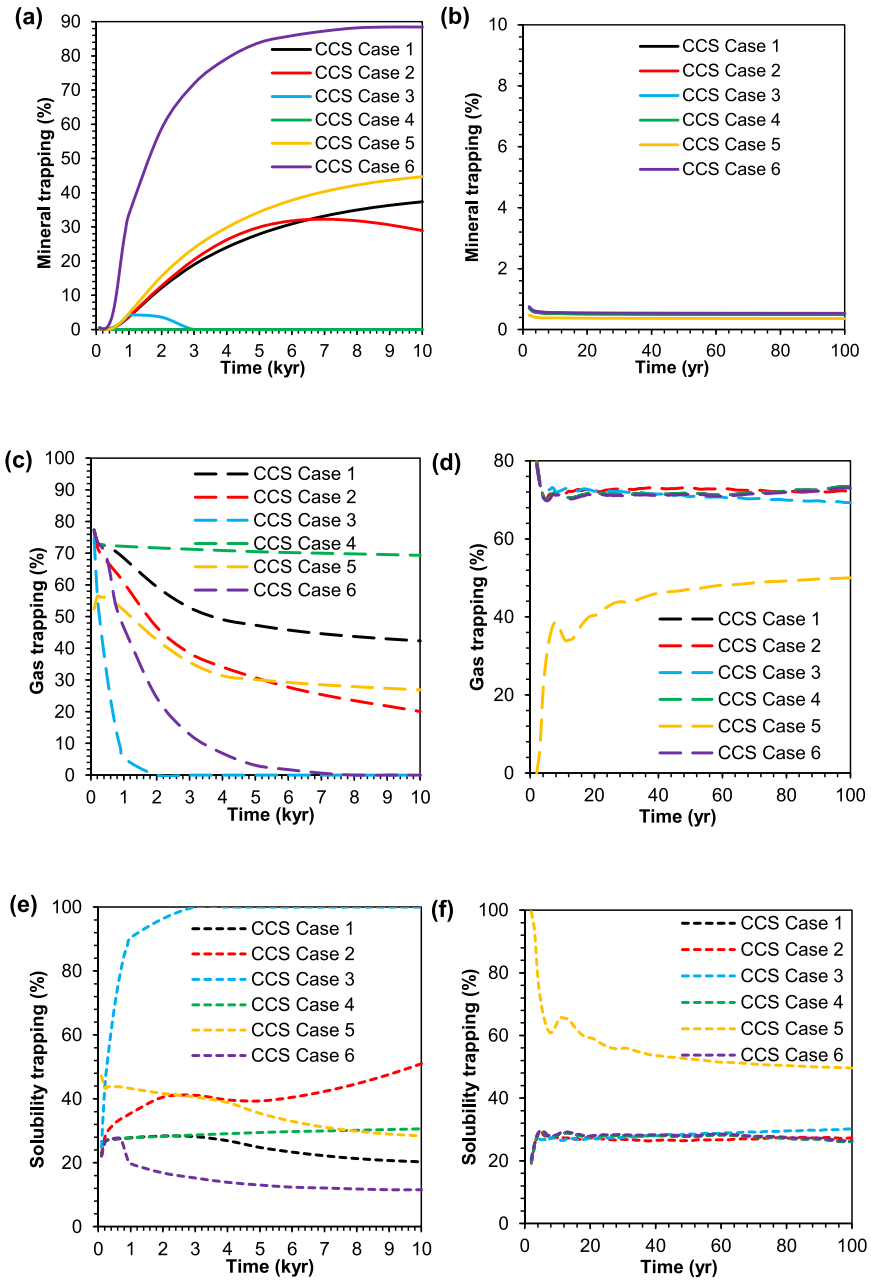

Fig. 5. Percentage of (a) and (b) mineral trapping, (c) and (d) gas trapping, and (d) and (f) solubility trapping as a function of time in the simulated domain in CCS Cases 1-6. (b), (d) and (f) are for the first 100 yr.

(X = 5650 m and Z = 1810 m as indicated by the white star on Fig. 3e) to investigate the projected solution chemistry of the Base Case as a function of time. In the Base Case, the reaction path began in the albite stability field, moving towards the albite-dawsonite-kaolinite three-phase triple point and entering the dawsonite stability field at 0.1 Myr, and then moving along the kaolinite-dawsonite boundary towards higher log(fCO_2) and lower log(aNa^+/aH^+) (Fig. 7a). Almost no change in both log(aNa^+/aH^+) and log(fCO_2) occurred between 1 – 15 Myr.

For CO_2 injection with a groundwater flow of 0.1 m/yr (CCS Case 2), the reaction path also began in the albite stability field, crossing the albite-kaolinite boundary to enter the kaolinite stability field at 200 yr. The solution chemistry moved towards the dawsonite stability field from 200 yr to 1 kyr but migrated back towards the albite stability field along the dawsonite-kaolinite and albite-kaolinite boundaries between 1 kyr and 10 kyr. It took ~0.1 Myr to move out of the albite stability field and enter the dawsonite stability field in the Base Case, but only ~1 kyr in CCS Case 2. This acceleration arises in comparison with the Base Case because CO_2 gas-phase dissolution and dawsonite precipitation are controlled mainly by the slow density-driven flow in the latter.

The dawsonite stability field decreases with increasing temperature (Figs. 7b-e). Dawsonite is stable when both (Na^+/H^+) activity and CO_2 fugacity are high, but such conditions are rare in regional saline aquifers. Figs. 7b-e show that all listed formation waters lie outside the dawsonite stability zone (the green circles). This potentially explains the uncommon occurrence of dawsonite; although it can form where CO_2 fugacity is high, the persistence of the latter is unusual.

In **SI Section S8**, we summarize the geological and geochemical conditions of natural dawsonite-bearing CO_2 reservoirs (Sites 1-10 in Figs. 7b-e) to study the stability and long-term conditions required for dawsonite preservation. Generally, a magmatic mantle-CO_2 source is assumed, and in the Hailar basin example, its preservation for up to 110 myr is possible (Gao et al., 2009; Gao, 2007). pH values range between 5

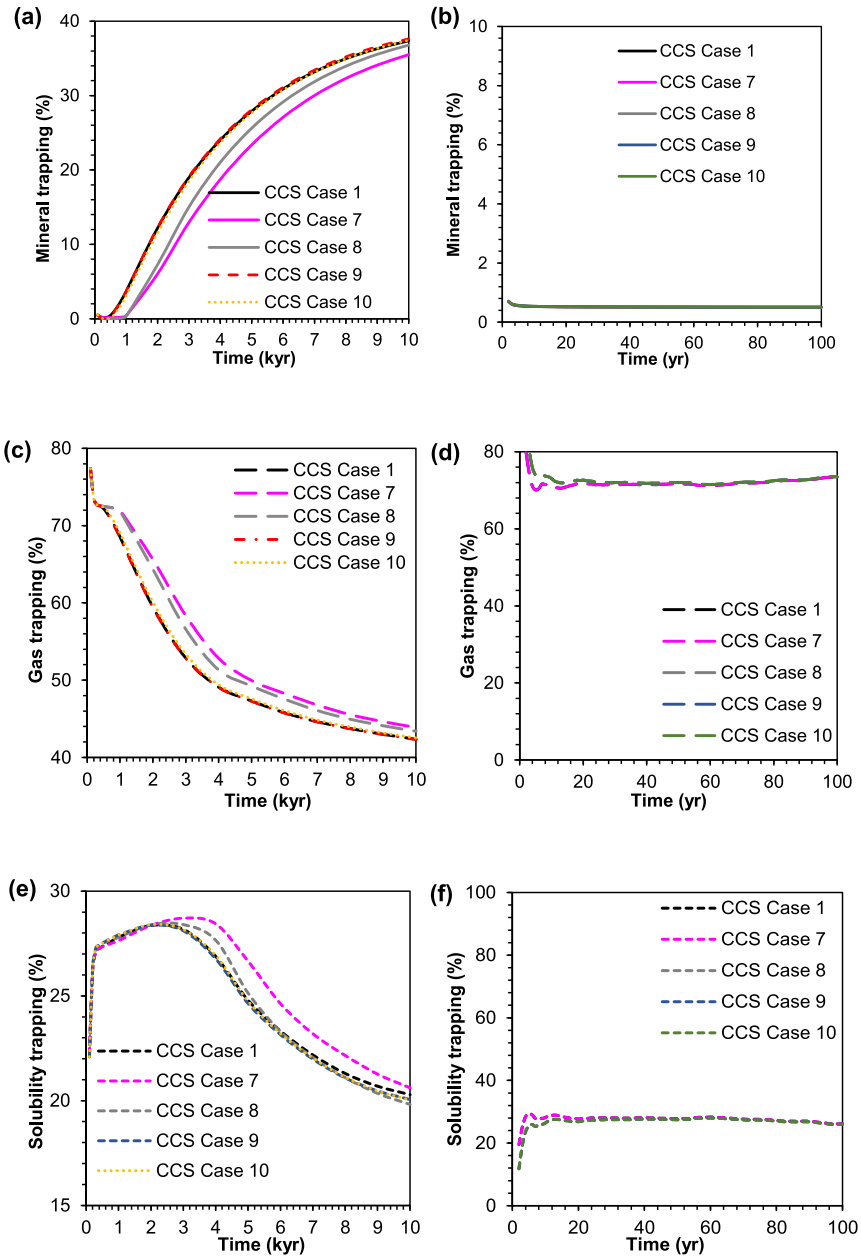

Fig. 6. Percentage of (a) and (b) mineral trapping, (c) and (d) gas trapping, and (d) and (f) solubility trapping as a function of time in the simulated domain in CCS Cases 1 and 7-10. (b), (d) and (f) are for the first 100 yr.

and 7. The solution chemistries (log (fCO_2) and log(aNa^+/aH^+) in the albite-dawsonite-kaolinite phase diagrams are all within the dawsonite stability field (blue triangles in Figs. 7b-e). These sites typically boast relatively closed hydrodynamic conditions (many are isolated in domes). Dawsonite-bearing natural CO_2 reservoirs commonly occur in sedimentary rocks with Na-rich feldspars (albite or oligoclase) (Comerio et al., 2014), relatively low local groundwater flow velocities, and in the presence of a CO_2 gas phase. Should any of these prerequisites diminish, dawsonite could destabilize and eventually disappear through a kinetically controlled process? Higgs et al. (2015) and Gaus et al. (2005) found that dawsonite does not exist in high CO_2 wells (98% CO_2 in the Otway Basin, Australia and 97-99% CO_2 at Montmiral, France) where Na-rich feldspar has been exhausted. The dissolution of dawsonite between 10-15 Myr in the Base Case of this study is also due to the depletion of albite.

Dawsonite is a major potential sink for CO_2 in natural CO_2 reservoirs and operated or planned CCS sites worldwide. In some proposed sites in Figs. 7 and 8, geologic conditions are suitable for dawsonite precipitation. Almost all sites contain Na-rich brine, and some have >3% Na-rich feldspar (Table 2). Dawsonite precipitation is less favorable with either Ca-, Mg-, and Fe-rich mineralogy or Ca-, Mg-, and Fe-rich formation water (e.g., sites 1, 2, 5, 6, 8-10, 13, 15, 19, 21, 23, 27, 29, 32-34, 36, 37, 42, and 44 in Table 2; about 44.7% of total sites investigated).

Except for dawsonite-bearing natural CO_2 reservoirs, all *in situ* brines before CO_2 injection at the proposed sites (black diamonds) lie outside the dawsonite stability field (Fig. 7). CO_2 injection would increase CO_2 fugacity, displacing the brine chemistry to the right and into the dawsonite stability field, thereby leading to dawsonite precipitation (e.g., the reaction path of CCS Case 2). Although thermodynamics and kinetics confirm previous model predictions of dawsonite precipitation in the literature, we also predict that dawsonite will dissolve when destabilizing native brines return. The tendency in CCS Case 2 to exit the dawsonite stability field indicates the potential instability of dawsonite in the system. Nevertheless, dawsonite's ephemeral presence will buffer

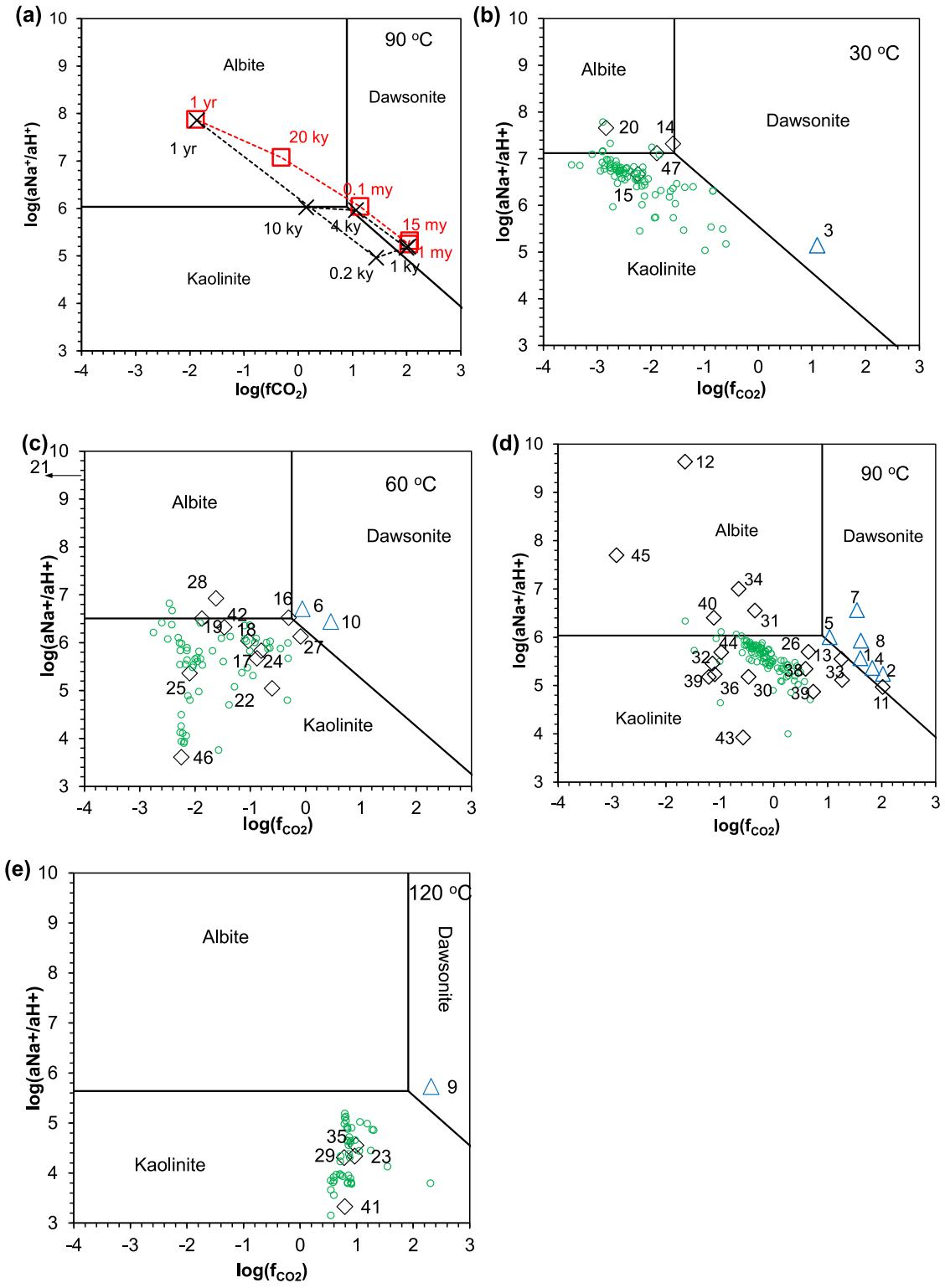

Fig. 7. Activity diagrams for albite, dawsonite, and kaolinite. (a) Modeled reaction paths in this study. Arrows show the reaction path evolution. (b-e) At 30, 60, 90 and 120 °C, respectively. Red squares indicate the projected solution chemistry of the Base Case as a function of time at the point X = 5650 m, Z = 1810 m (as indicated by the white star on Fig. 3e). Black crosses indicate the solution chemistry of CCS Case 2 as a function of time at X = 7450 m, Z = 1700 m (as indicated by the white star on Fig. S7-1c). Dashed lines denote reaction paths. Green circles are formation water samples from U.S. Geological Survey National Produced Waters Geochemical Database at relevant temperatures (Blondes et al., 2018). To correct for aqueous sample CO_2 degassing, CO_2(g) in the waters was incrementally augmented, until attainment of equilibrium with calcite at reservoir temperature, following Palandri and Reed (2001). Black open diamonds denote the projected *in situ* brine chemistries before CO_2 injection from CCS projects, natural analogues, and saline aquifers around the world, and blue triangles are dawsonite-bearing CO_2 reservoirs. Locations and characteristics of the numbered sites are given in **SI Section 8**.

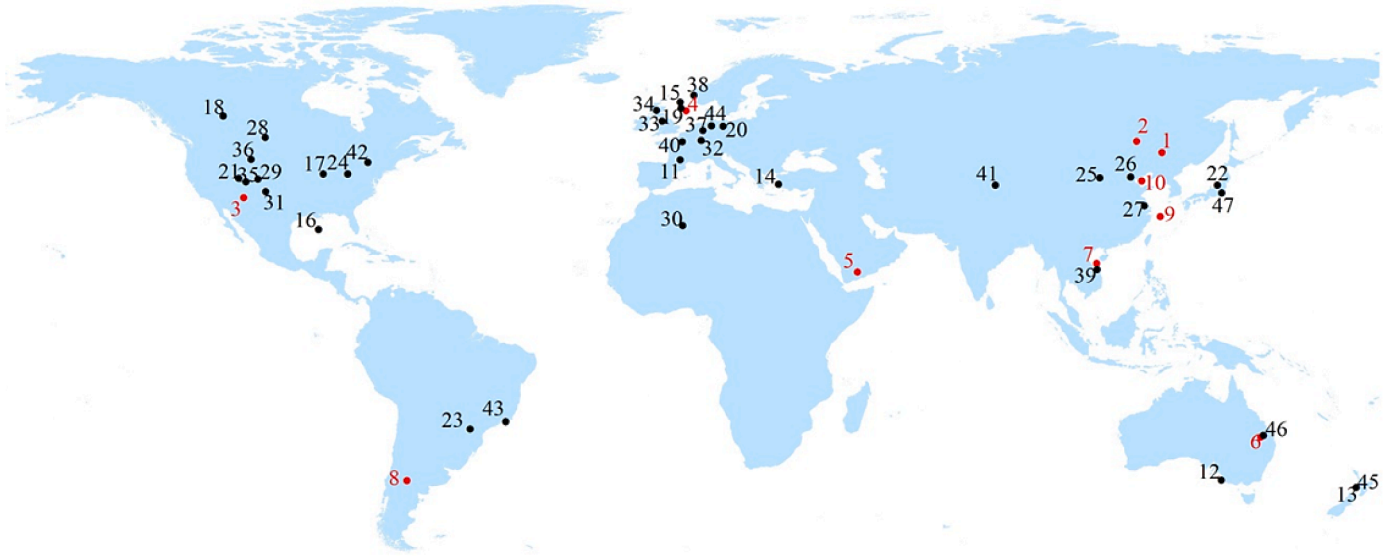

Fig. 8. Distribution of the sites investigated in this study (listed in Table 2 and detailed in **SI**) on a global map. Red dots (1-10) denote dawsonite-bearing natural CO_2 reservoirs.

the CO_2 plume.

4.5. Issues Relating to Dawsonite Nucleation and Growth

The central argument of this paper is that dawsonite precipitation in sedimentary formations containing sodic-rich feldspars could make a substantial contribution towards isolating carbon dioxide from the atmosphere. The argument is supported by simulating its formation in a representative and well-studied deposit of naturally occurring secondary dawsonite in the Hailar basin of China and showing that similar processes operate during accelerated CO_2 injection. This proposition is, however, controversial. Over the last 25 years, many reactive transport simulations have reported dawsonite as a secondary precipitate, yet it has never been observed to form during analogous laboratory or field tests, e.g. see Bateman et al. (2005). Furthermore, in several naturally-occurring high-pressure CO_2 reservoirs in sedimentary formations where dawsonite formation would be expected, it is either not observed or occurs only as a minor constituent, e.g. see Pawels et al. (2007) and Wilkinson et al. (2009). This has led to a general skepticism regarding its value for trapping CO_2, especially when forming in competition with divalent carbonates, and further, when its persistence would supposedly depend on a sustained elevated P_{CO2}. The key question then is whether sufficient dawsonite can form and persist long enough in suitable formations for it to be considered as a viable CO_2 sequestering agent.

Although dawsonite thermodynamic properties are sufficiently well known not to limit thermodynamic modeling, *c.f.* Ferrante et al. (1976), Bénézeth et al. (2007), other aspects relating to dawsonite formation and persistence remain unresolved or are insufficiently characterized, and these are summarized here; (1) Laboratory and field tests to investigate CO_2 sequestration in sedimentary formations were generally not designed to investigate, or were of insufficient duration to permit observable dawsonite formation and cannot be used to refute its potential value as a CO_2 mineral trapping agent; (2) Current reactive transport simulators possess a number of deficiencies relating to the algorithns used to model the kinetics of heterogeneous reactions between minerals, therby limiting their ability to make quantitative predictions relating to the timing of mineral precipitation, including dawsonite, as noted by Pham et al. (2011), and whose modeling substantiates the claim given in (1); (3) The stability field of dawsonite in relation to participating components of rock-forming minerals, divalent carbonates, CO_2 and H_2O in P, T, X space has not been attempted, and therefore neither its relationship to divalent carbonates nor the limits of its stability are known (Sirbescu and Nabelek, 2003); (4) Field evidence shows that dawsonite crystallizes as open radiating or dense spherulitic aggregates of fibrous crystals, e.g. see Gao et al. (2009), implying that heterogeneous nucleation and growth took place only after significant levels of supersaturation had been attained (Sunagawa, 1999), which in turn suggests that a long induction times between initial CO_2 injection and the critical threshold where heterogeneous nucleation of dawsonite could occur. Indeed, if only low levels of initial supersaturation were achieved, it might never form; (5) Very few laboratory experiments to quantify the kinetics of heterogeneous dawsonite nucleation and growth have been made, e.g, see Smirnov and Lobanova (1965), but the conditions differ substantially from those expected in the field; (6) The application of classical nucleation theory (CNT) as an adequate framework for interpreting nucleation and growth has recently been challenged (Whitehead et al., 2019); (7) Given that the aqueous concentrations of the chemical components participating in dawsonite precipitation depart strongly from stoichiometry, especially with respect to alumina, its nucleation and initial growth would lead to an immediate collapse in the level of supersaturation, and subsequent growth would almost certainly be dominated only by a screw dislocation process (Nielsen and Christoffersen, 1982). In that respect, the nucleation and precipitation of dawsonite in the field likely reflects the instantaneous or "burst" nucleation hypothesis first described in terms of CNT by La Mer et al. (1950) and applied to describe the nucleation and growth of colloidal sulfur. However, as noted by Whitehead et al. (2019), the actual La Mer equation is inconsistent with experimental kinetic data; (8) No detailed measurements of dawsonite crystal growth have been made. The use of dissolution data to predict growth using TST is unlikely to be meaningful; (9) The radiating fibrous nature of dawsonite implies an essentially one-dimensional growth mechanism. Theory to explain both the initial polynuclear growth front nucleation to account for the radiating or spherulitic habit has not been developed, although phase-field modeling has been moderately successful in replicating the process (Gránásy et al., 2005, 2021); (10) Theory explaining one-dimensional mineral growth in aqueous solution, as is characteristic of naturally-occurring dawsonite in sedimentary arkosic formations, has not been attempted, although the tools to do so are available, e.g., see Jolivet et al. (2004) who show how acidity and ionic strength can affect the morphology of nano-sized metal oxide particles. More recent studies on the morphology and surface properties of boehmite using density functional theory, e.g., Prange et al., (2018) suggest potential

Table 2
Mineralogical and formation water characteristics of some of the proposed sites for CCS[a]

Sites	Mineralogy[b]		Formation water[c]	
	Na-rich	Ca, Mg, Fe-rich	Na-rich	Ca, Mg, Fe-rich
1. Songliao Basin, China	•			
2. Hailar Basin, China	•			
3. Springerville – St Johns Field, Arizona, USA	•	•		
4. Rotliegend Formation, southern North Sea			•	•
5. Shabwa Basin, Yemen	•		•	
6. Bowen-Gunnedah-Sydney basin	•		•	
7. Yinggehai Basin, South China Sea	•	•	•	
8. Patagonia, Agentina	•		•	
9. East China Sea Basin, China	•		•	
10. Bohai Bay Basin, China	•		•	
11. Montmiral, France		•	•	
12. Otway Basin, Australia	•	•	•	
13. Kapuni field, New Zealand			•	
14. Messokampos, Greece	•	•		
15. Sleipner, Norway	•		•	
16. Frio "C" Fm., Texas, USA	•	•	•	
17. Mt. Simon sandstone, IL, IN, KY, USA	•		•	•
18. Glauconitic Sandstone, Alberta Basin, Canada		•	•	
19. Bunter sandstone, UK North Sea	•		•	
20. Ketzin, Northeast German Basin	•	•	•	
21. White Rim sandstone, UT, USA			•	
22. Nagoaka Sandstone, Japan	•	•		
23. Parana Basin, Argentina			•	
24. Rose Run aquifer, Ohio			•	•
25. Shenhua CCS pilot, Ordos Basin, China	•	•	•	•
26. Bonan Sag, eastern Bohai Bay Basin, China	•	•	•	
27. Huangqiao, Jiangsu, China	•		•	
28. Weyburn reservoir, Canada		d	•	
29. Navajo sandstone, Colorado, USA			•	
30. In Salah, Algeria		•	•	•
31. Bravo Dome, New Mexico, USA		•	•	
32. Adamswiller sandstone, Paris Basin, France			•	
33. Miller field, North Sea, UK			•	
34. Magnus field, North Sea, UK			•	
35. Paradox Valley, Colorado		d	•	•
36. Tensleep formation, Wyoming, USA			•	
37. Westphalian sandstones, Campine Basin, Belgium			•	
38. Snøhvit, SW Barents Sea, Norway			•	•
39. Da Nang Basin, offshore Vietnam		d	•	
40. Vert le Grand, Paris basin, France			•	•
41. Tarim Basin, China		d		•
42. Arkose and Silurian Maplewood shale, USA			•	
43. Rio-Bonito formation, Brazil			•	•
44. North German Basin			•	
45. Kapuni field, New Zealand		•	•	
46. Surat Basin, Australia		•		
47. Kazusa Group, Tokyo Bay	•	•		

[a] Detailed information of the numbered sites is listed in **SI Section S8**. The sites are also shown in Figures 6 and 7. Sites in red text (1-10) are dawsonite-bearing natural CO_2 reservoirs.
[b] With >~3% of the mineral of interest.
[c] With >~0.3 mol/kg H_2O of Na or >~0.1 mol/kg H_2O of divalent cations.
[d] Carbonate reservoirs contain mainly calcite and dolomite.

methodologies for explaining dawsonite growth and morphology.

Hellevang and his co-workers, e.g., Hellevang et al. (2011) and Pham et al. (2011) were keenly aware of many of the issues relating to the stability and kinetics of dawsonite nucleation and growth, and used CNT (Nielsen, 1964; Walton, 1967) to describe the heterogeneous nucleation of dawsonite and Burton-Cabrera-Frank (BCF) theory to simulate screw dislocation growth (Burton et al., 1951). However, Pham et al. (loc. cit.) admit that further laboratory experimental studies of heterogeneous nucleation and growth are needed, not only in relation to dawsonite, but also to other divalent carbonates. Recent research developments in physical chemistry and materials science reinforces the urgency of this need.

Scoping studies incorporating developments in CNT by Liu (2000) to quantify bounding estimates to the critical parameters defining dawsonite heterogeneous nucleation and growth under relevant field conditions, together with a suitable thermodynamic evaluation of the dawsonite stability field under similar conditions could provide a basis for designing confirmatory laboratory experiments. However, the results of such experiments should also be used to test the validity of CNT in that context. This approach should contribute, not only towards opening further opportunities for CCS, but also advance our understanding of the science of heterogeneous nucleation and growth of natural and synthetic materials showing a fibrous crystal habit.

The reactive transport simulations presented in this paper highlight dawsonite formation under various CO_2 injection and hydrologic conditions using the current state-of-the-art together with optional refinements or adjustments to account, at least in part, for current deficiencies in such modeling. However, the authors readily concede that further refinements will increase confidence in their findings and conclusions, and hopefully narrow the uncertainty relating to the timing of dawsonite formation following CO_2 injection.

5. Implications

Dawsonite mineral trapping is thermodynamically favored when CO_2 injection for CCS generates a high CO_2 fugacity, and where most operational and proposed storage formations contain >3% Na-feldspars (Table 2). Although unlikely to be a permanent sink for injected CO_2 in a hydraulically open system, it can be significant over the CCS time scale. Even though temporary, CO_2 trapping by dawsonite over thousands of years would be beneficial, as it would decrease the risks associated with CO_2 leakage to the ground surface or overlying drinking water aquifers. Dawsonite trapping should therefore be an important consideration for selecting sites abundant in Na-rich feldspar, Na concentration in the formation water, and regional groundwater flow rates. WAG injection should be considered in injection design and practice, as it could further enhance solubility trapping and promote dawsonite precipitation.

Reservoirs or saline aquifers with minerals or formation water containing abundant divalent Ca, Mg, and Fe are preferred CCS sites, as they can trap CO_2 in carbonate minerals, e.g., calcite, magnesite, siderite, and ankerite. This category includes divalent-cation-rich formation waters, e.g., those associated with evaporates and dolomites, or resulting from albitization, thermal or bacterial sulfate reduction of anhydrite or gypsum, or fluid-mafic rock interaction involving divalent-cation-rich silicate minerals, e.g., olivine, pyroxene, and calcium-rich plagioclase in the rock fragments.

Because dawsonite is favorable as a temporary sink, we also propose consideration of saline aquifers with minerals or formation water providing elevated $\log((Na^+)/(H^+))$ activities. Thus, about 45% of the sites in Table 2 could also be considered for site selection with this criterion. A Na-rich brine is significant because it could affect mineral and solubility trapping. Na-rich formation waters could be associated with evaporation, halite dissolution, and/or gravity segregation, and where Na-rich silicate minerals are predominantly Na-rich feldspars.

The current version of Carbon Storage Atlas by the U.S. Department of Energy considers only the volume in assessing the carbon storage

potentials of saline aquifers and relates mainly to the short-term structural and residual trapping of CO_2 under supercritical conditions. We recommend also accounting for the quantity and concentrations of the divalent-cation-rich and Na-rich formation minerals or saline aquifers for the potential long-term safety of carbon storage in future editions of the Carbon Storage Atlas.

Author contributions

P.L. and G.Z. conceived the study and implemented the model. G.Z. and Y. H. conducted the numerical modeling, analyzed and interpreted the data. P.L., J.A., and C.Z. contributed to the writing and revision of the manuscript.

Declaration of Competing Interest

The authors have no conflict of interest to report.

Acknowledgments

CZ's contribution to this work was partially supported by the U.S. NSF grant EAR-1926734, the Faculty Research Support Program at Indiana University, and the Haydn Murray chair endowment, and donors of American Chemical Society – Petroleum Research Fund for grant #57727-ND2. GRZ would like to thank the Everest Scientific Research Program grant 2020ZF11405 and the Science and Technology Departement of Sichuan Province grant 2021JDTD0013for partial support of this research. Lawrence Berkeley National Laboratory is acknowledged for donating TOUGHREACT V3.0-OMP-ECO2N software to Indiana University. We thank Anne Hereford for her editorial assistance.

Supplementary materials

Supplementary material associated with this article can be found, in the online version, at doi:10.1016/j.ijggc.2022.103733.

References

Aagaard, P., Helgeson, H.C., 1982. Thermodynamic and kinetic constraints on reaction rates among minerals and aqueous solutions. I. Theoretical considerations. Am. J. Sci. 282, 237–285.

Alekseyev, V.A., Medvedeva, L.S., Prisyagina, N.I., Meshalkin, S.S., Balabin, A.I., 1997. Change in the dissolution rates of alkali feldspars as a result of secondary mineral precipitation and approach to equilibrium. Geochim. Cosmochim. Acta 61 (6), 1125–1142.

Audigane, P., Gaus, I., Czernichowski-Lauriol, I., Pruess, K., Xu, T., 2007. Two-dimensional reactive transport modeling of CO_2 injection in a saline aquifer at the Sleipner site, North Sea. Am. J. Sci. 307, 974–1008.

Bachu, S., Gunter, W.D., Perkins, E.H., 1994. Aquifer disposal of CO_2: hydrodynamic and mineral trapping. Energy Convers. Manage. 35 (4), 269–279.

Baker, J.C., Bai, G.P., Hamilton, P.J., Golding, S.D., Keene, J.B., 1995. Continental-scale magmatic carbon dioxide seepage recorded by dawsonite in the Bowen-Gunnedah-Sydney Basin system, eastern Australia. J. Sediment. Res. 65 (3a), 522–530.

Bateman, K., Turner, G., Pearce, J.M., Noy, D.J., Birchall, D., Rochelle, C.A., 2005. Large-scale column experiment: study of CO_2, porewater, rock reactions and model test case. Oil & Gas Sci. Technol. 60 (1), 161–175.

Bénézeth, P., Palmer, D.A., Anovitz, L.M., Horita, J., 2007. Dawsonite synthesis and reevaluation of its thermodynamic properties from solubility measurements: Implications for mineral trapping of CO_2. Geochim. Cosmochim. Acta 71 (18), 4438–4455.

Blondes, M.S., Gans, K.D., Engle, M.A., Kharaka, Y.K., Reidy, M.E., Saraswathula, V., Thordsen, J.J., Rowan, E.L., & Morrissey, E.A., (2018). U.S. Geological Survey National Produced Waters Geochemical Database (ver. 2.3, January 2018): U.S. Geological Survey data release, https://doi.org/10.5066/F7J964W8.

Burton, W.K., Cabrera, N., Frank, F.C., 1951. The growth of crystals and the equilibrium structure of their surfaces. R. Soc. Lond. Philos. Trans. 243, 299–358.

Cantucci, B., Montegrossi, G., Vaselli, O., Tassi, F., Quattrocchi, F., Perkins, E.H., 2009. Geochemical modeling of CO_2 storage in deep reservoirs: The Weyburn Project (Canada) case study. Chem. Geol. 265 (1-2), 181–197.

Comerio, M., Morosi, M.E., Tunik, M., Paredes, J.M., Zalba, P.E., 2014. The role of telogenetic injection of magmatically derived CO_2 in the formation of dawsonite from the Castillo Formation, Chubut Group, Patagonia, Argentina. The Canadian Mineralogist 52 (3), 513–531.

Coudrain-Ribstein, A., Gouze, P., de Marsily, G., 1998. Temperature-carbon dioxide partial pressure trends in confined aquifers. Chem. Geol. 145 (1-2), 73–89.

Cseresznyés, D., Czuppon, G., Király, C., Demény, A., Györe, D., Forray, V., Kovács, I., Szabó, C., Falus, G., 2021. Origin of dawsonite-forming fluids in the Mihályi-Répcelak field (Pannonian Basin) using stable H, C and O isotope compositions: Implication for mineral storage of carbon-dioxide. Chem. Geol. 584, 120536.

Du, Y.H., 1982. Secondary dawsonite in Shengli oil field, China. Scientia Geologica Sinica (4), 434–437.

Ferrante, M.J., Stuve, J.M., Richardson, D.W., 1976. Thermodynamic data for synthetic dawsonite (Rept Inv. 8129). US Department of the Interior. US Bureau of Mines, p. 13.

Gao, Y., 2007. Thermal convection diagenesis of reservoir sandstone of magmatic CO_2 pool-Taking the Wuerxun Depression. Hailaer Basin for example. Jilin University, Changchun, China, p. 169.

Gao, Y., Liu, L., Hu, W., 2009. Petrology and isotopic geochemistry of dawsonite-bearing sandstones in Hailaer basin, northeastern China. Appl. Geochem. 24, 1724–1738.

Gaus, I., Azaroual, M., Czernichowski-Lauriol, I., 2005. Reactive transport modelling of the impact of CO_2 injection on the clayey cap rock at Sleipner (North Sea). Chem. Geol. 217, 319–337.

Gránásy, L., Pusztai, T., Tegze, G., Warren, J.A., Douglas, J.F., 2005. Growth and form of spherulites. Phys. Rev. E 72 (1), 011605.

Gránásy, L., Rátkai, L., Tóth, G.I., Gilbert, P.U., Zlotnikov, I., Pusztai, T., 2021. Phase-Field Modeling of Biomineralization in Mollusks and Corals: Microstructure vs Formation Mechanism. JACS Au 1, 1014–1033.

Hellevang, H., Aagaard, P., Oelkers, E.H., Kvamme, B., 2005. Can dawsonite permanently trap CO_2? Environ. Sci. Technol. 39, 8281–8287.

Hellevang, H., Declercq, J., Kvamme, B., Aagaard, P., 2010. The dissolution rates of dawsonite at pH 0.9 to 5 and temperatures of 22, 60 and 77 C. Appl. Geochem. 25 (10), 1575–1586.

Hellevang, H., Declercq, J., Aagaard, P., 2011. Why is dawsonite absent in CO_2 charged reservoirs? Oil & Gas Science and Technology–Revue d'IFP Energies Nouvelles 66 (1), 119–135.

Hellevang, H., Aagaard, P., Jahren, J., 2014. Will dawsonite form during CO_2 storage? Greenhouse Gases Sci. Technol. 4 (2), 191–199.

Higgs, K.E., Haese, R.R., Golding, S.D., Schacht, U., Watson, M.N., 2015. The Pretty Hill Formation as a natural analogue for CO_2 storage: An investigation of mineralogical and isotopic changes associated with sandstones exposed to low, intermediate and high CO_2 concentrations over geological time. Chem. Geol. 399, 36–64.

IPCC, 2005. Special report on carbon dioxide capture and storage. Intergovernmental Panel on Climate Change.

Johnson, J.W., Nitao, J.J., Knauss, K.G., 2004. Reactive transport modelling of CO_2 storage in saline aquifers to elucidate fundamental processes, trapping mechanisms and sequestration partitioning. Geological Society, London, Special Publications 233 (1), 107–128.

Jolivet, J.P., Froidefond, C., Pottier, A., Chanéac, C., Cassaignon, S., Tronc, E., Euzen, P., 2004. Size tailoring of oxide nanoparticles by precipitation in aqueous medium. A semi-quantitative modelling. J. Mater. Chem. 14 (21), 3281–3288.

Király, C., Sendula, E., Szamosfalvi, Á., Káldos, R., Kónya, P, Kovács, I.J., Füri, J., Bendő, Z., Falus, G., 2018. The relevance of dawsonite precipitation in CO_2 sequestration in the Mihályi-Répcelak area, NW Hungary. Geological Society, London, Special Publications 435 (1), 405–418.

Lasaga, A.C., 1981a. Rate laws of chemical reactions. In: Lasaga, A.C., Kirkpatrick, R.J. (Eds.), Kinetics of Geochemical Processes, 8. Mineralogical Society of America, Washington, DC, pp. 1–68.

Lasaga, A.C., 1981b. Transition state theory. In: Lasaga, A.C., Kirkpatrick, R.J. (Eds.), Kinetics of Geochemical Processes, 8. Mineralogical Society of America, Washington, DC, pp. 135–169.

Li, F.L., Li, W.S., 2016. Controlling factors for dawsonite diagenesis: a case study of the Binnan Region in Dongying Sag, Bohai Bay Basin, China. Aust. J. Earth Sci. 63 (2), 217–233.

Li, F., Li, W., Yu, Z., Liu, N., Yang, H., Liu, L., 2017. Dawsonite occurrences related to the age and origin of CO_2 influx in sandstone reservoirs: A case study in the S ongliao B asin, NE C hina. Geochem. Geophys. Geosyst. 18 (1), 346–368.

Li, F., Cao, Y., Li, W., Zhang, L., 2018. CO_2 mineral trapping: Hydrothermal experimental assessments on the thermodynamic stability of dawsonite at 4.3 Mpa pCO_2 and elevated temperatures. Greenhouse Gases Sci. Technol. 8 (1), 77–92.

Liu, X.Y., 2000. Generic progressive heterogeneous processes in nucleation. Langmuir 16 (18), 7337–7345.

Liu, F., Lu, P., Zhu, C., Xiao, Y., 2011. Coupled reactive flow and transport modeling of CO_2 sequestration in the Mt. Simon sandstone formation, Midwest USA. Int. J. Greenhouse Gas Control 5 (2), 294–307.

Liu, N., Liu, L., Qu, X., Yang, H., Wang, L., Zhao, S., 2011. Genesis of authigene carbonate minerals in the Upper Cretaceous reservoir, Honggang Anticline, Songliao Basin: A natural analogue for mineral trapping of natural CO_2 storage. Sediment. Geol. 237, 166–178.

Lu, P., Luo, P., Zhang, G., Zhang, S., Zhu, C., 2020. A mineral-water-gas interaction model of pCO_2 as a function of temperature in sedimentary basins. Chem. Geol. 558, 119868.

Ming, X.R., Liu, L., Yu, L., Bai, H.G., Yu, Z.C., Liu, N., Yang, H.X., Wang, F.G., Li, B.X., 2017. Thin-film dawsonite in Jurassic coal measure strata of the Yaojie coalfield, Minhe Basin, China: A natural analogue for mineral carbon storage in wet supercritical CO_2. Int. J. Coal Geol. 180, 83–99.

Moore, J., Adams, M., Allis, R., Lutz, S., Rauzi, S., 2005. Mineralogical and geochemical consequences of the long-term presence of CO_2 in natural reservoirs: an example from the Springerville–St. Johns Field, Arizona, and New Mexico, USA. Chem. Geol. 217 (3-4), 365–385.

Nielsen, A.E., 1964. The Kinetics of Precipitation. MacMillan, New York, p. 153.
Nielsen, A.E., Christoffersen, J., 1982. The mechanisms of chrystal [sic] growth and dissolution. In: Nancollas, G.H. (Ed.), Biological mineralization and demineralization. Springer-Verlag, Berlin, Heidelberg, pp. 37–77.
Okuyama, Y., Todaka, N., Sasaki, M., Ajima, S., Akasaka, C., 2013. Reactive transport simulation study of geochemical CO_2 trapping on the Tokyo Bay model–With focus on the behavior of dawsonite. Appl. Geochem. 30, 57–66.
Palandri, J.L., Reed, M.H., 2001. Reconstruction of in situ composition of sedimentary formation waters. Geochim. Cosmochim. Acta 65 (11), 1741–1767.
Pauwels, H., Gaus, I., Le Nindre, Y.M., Pearce, J., Czernichowski-Lauriol, I., 2007. Chemistry of fluids from a natural analogue for a geological CO_2 storage site (Montmiral, France): lessons for CO2–water–rock interaction assessment and monitoring. Appl. Geochem. 22 (12), 2817–2833.
Pham, V.T.H., Lu, P., Aagaard, P., Zhu, C., Hellevang, H., 2011. On the potential of CO_2–water–rock interactions for CO_2 storage using a modified kinetic model. Int. J. Greenhouse Gas Control 5 (4), 1002–1015.
Prange, M.P., Zhang, X., Bowden, M.E., Shen, Z., Ilton, E.S., Kerisit, S.N., 2018. Predicting surface energies and particle morphologies of boehmite (γ-AlOOH) from density functional theory. The Journal of Physical Chemistry C 122 (19), 10400–10412.
Qu, X., Zhang, Y., Li, Q., Du, T., Li, Y., 2022. Geological features and occurrence conditions of dawsonite as a main Carbon-Fixing mineral. Alexandria Eng. J. 61 (4), 2997–3011.
Shabani, B., Lu, P., Kammer, R., Zhu, C., 2022. Effects of Hydrogeological Heterogeneity on CO_2 Migration and Mineral Trapping: 3D Reactive Transport Modeling of Geological CO_2 Storage in the Mt. Simon Sandstone, Indiana, USA. Energies 15 (6), 2171.
Sirbescu, M.L.C., Nabelek, P.I., 2003. Dawsonite: an inclusion mineral in quartz from the Tin Mountain pegmatite, Black Hills, South Dakota. Am. Mineral. 88 (7), 1055–1059.
Smirnov, M.N, Lobanova, E.V., 1965. Formation of sodium hydroalumocarbonate under hydrothermal conditions in the interaction of hydrargillite with sodium bicarbonate. Issledovaniia v Oblasti Khimii i Tekhnologii Mineral'nykh Soleĭ i Okislov : Sbornik Stateĭ. Nauka, Leningrad, pp. 128–135 [In Russian].
Snæbjörnsdóttir, S.Ó., Oelkers, E.H., Mesfin, K., Aradóttir, E.S., Dideriksen, K., Gunnarsson, I., Gunnlaugsson, E., Matter, J.M., Stute, M., Gislason, S.R., 2017. The chemistry and saturation states of subsurface fluids during the in situ mineralisation of CO_2 and H_2S at the CarbFix site in SW-Iceland. Int. J. Greenhouse Gas Control 58, 87–102.
Sunagawa, I., 1999. Growth and morphology of crystals. FORMA-TOKYO 14 (1/2), 147–166.
Takaya, Y., Wu, M., Kato, Y., 2019. Unique Environmental Conditions Required for Dawsonite Formation: Implications from Dawsonite Synthesis Experiments under Alkaline Conditions. ACS Earth Space Chem. 3 (2), 285–294.
Uysal, I.T., Golding, S.D., Bolhar, R., Zhao, J.X., Feng, Y.X., Baublys, K.A., Greig, A., 2011. CO_2 degassing and trapping during hydrothermal cycles related to Gondwana rifting in eastern Australia. Geochim. Cosmochim. Acta 75 (19), 5444–5466.
Walton, A.G., 1967. The Formation and Properties of Precipitates. Interscience Publishers, New York, p. 232.
Whitehead, C.B., Özkar, S., Finke, R.G., 2019. LaMer's 1950 model for particle formation of instantaneous nucleation and diffusion-controlled growth: a historical look at the model's origins, assumptions, equations, and underlying sulfur sol formation kinetics data. Chem. Mater. 31 (18), 7116–7132.
Wilkinson, M., Haszeldine, R.S., Fallick, A.E., Odling, N., Stoker, S.J., Gatliff, R.W., 2009. CO_2–mineral reaction in a natural analogue for CO_2 storage—implications for modeling. J. Sediment. Res. 79 (7), 486–494.
Wopfner, H., Höcker, C.F., 1987. The Permian Groeden Sandstone between Bozen and Meran (northern Italy), a habitat of dawsonite and nordstrandite. Neues Jahrbuch für Geologie und Paläontologie-Monatshefte 161–176.
Worden, R.H., 2006. Dawsonite cement in the Triassic Lam Formation, Shabwa Basin, Yemen: A natural analogue for a potential mineral product of subsurface CO_2 storage for greenhouse gas reduction. Mar. Pet. Geol. 23 (1), 61–77.
Xu, T., Apps, J.A., Pruess, K., 2004. Numerical simulation to study mineral trapping for CO_2 disposal in deep aquifer. Appl. Geochem. 19 (6), 917–936.
Xu, T., Apps, J.A., Pruess, K., 2005. Mineral sequestration of carbon dioxide in a sandstone–shale system. Chem. Geol. 217 (3-4), 295–318.
Xu, T., Kharaka, Y.K., Doughty, C., Freifeld, B.M., Daley, T.M., 2010. Reactive transport modeling to study changes in water chemistry induced by CO2 injection at the Frio-I Brine Pilot. Chem. Geol. 271 (3-4), 153–164.
Yang, G., Li, Y., Atrens, A., Liu, D., Wang, Y., Jia, L., Lu, Y., 2017. Reactive transport modeling of long-term CO2 sequestration mechanisms at the Shenhua CCS demonstration project, China. J. Earth Sci. 28 (3), 457–472.
Yu, M., Liu, L., Yu, Z., Liu, N., Yang, H., Qu, X., 2014. Dawsonite fixation of mantle CO_2 in the cretaceous Songliao Basin, Northeast China: a natural analogue for CO_2 mineral trapping in oilfields. Int. Geol. Rev. 56 (14), 1792–1812.
Yu, Z., Liu, L., Liu, K., Yang, S., Yang, Y., 2015. Petrological characterization and reactive transport simulation of a high-water-cut oil reservoir in the Southern Songliao Basin, Eastern China for CO2 sequestration. Int. J. Greenhouse Gas Control 37, 191–212.
Yu, L., Wu, K., Liu, L., Liu, N., Ming, X., Oelkers, E.H., 2020. Dawsonite and ankerite formation in the LDX-1 structure, Yinggehai basin, South China sea: An analogy for carbon mineralization in subsurface sandstone aquifers. Appl. Geochem. 120, 104663.
Zhang, G., Lu, P., Zhang, Y., Wei, X., Zhu, C., 2015. Effects of rate law formulation on predicting CO2 sequestration in sandstone formations. Int. J. Energy Res. 39 (14), 1890–1908.
Zhang, G., Lu, P., Wei, X., Zhu, C., 2016. Impacts of mineral reaction kinetics and regional groundwater flow on long-term CO_2 fate at Sleipner. Energy Fuels 30 (5), 4159–4180.
Zhang, G., Lu, P., Luo, P., Sonnenthal, E., Huang, Y., Zhu, C., 2019. Effects of natural gas acidic components on local porosity generation in a carbonate reservoir: Insights from reactive transport modeling. AAPG Bulletin 103, 2975–3001.
Zhang, G., Lu, P., Huang, Y., Li, G., Zhu, C., 2021. Investigation of mineral trapping processes based on coherent front propagation theory: A dawsonite-rich natural CO_2 reservoir as an example. Int. J. Greenhouse Gas Control 110, 103400.
Zhao, S., Liu, L., Liu, N., 2018. Petrographic and stable isotopic evidences of CO_2-induced alterations in sandstones in the Lishui sag, East China Sea Basin, China. Appl. Geochem. 90, 115–128.
Zhou, B., Liu, L., Zhao, S., Ming, X.-R., Oelkers, E.H., Yu, Z.-C., Zhu, D.-F., 2014. Dawsonite formation in the Beier Sag, Hailar Basin, NE China tuff: A natural analogue for mineral carbon storage. Appl. Geochem. 48, 155–167.
Zhu, H., Xu, T., Tian, H., Feng, G., Yang, Z., Zhou, B., 2019. Understanding of Long-Term CO_2-Brine-Rock Geochemical Reactions Using Numerical Modeling and Natural Analogue Study. Geofluids 2019, 1426061.